DELIVERABLE

FP7-ICT-2013-11-619456

Sitoga

SILICON CMOS COMPATIBLE TRANSITION METAL OXIDE TECHNOLOGY FOR BOOSTING HIGHLY INTEGRATED PHOTONIC DEVICES WITH DISRUPTIVE PERFORMANCE

SPECIFIC TARGETED RESEARCH PROJECTS			
Deliverable D3.5 BTO/Si Mach-Zehnder modulator compliant to specifications			
Delivery Date:	31/05/2016 (M30)	Date of submission:	04/07/2016
Start date of project:	01/12/2013 (M01)	Duration:	36 months
Lead Participant for this Deliverable			
Name:	IBM Research GmbH		
Contact Person:	Stefan Abel		
Address:	Säumerstrasse 4, CH-8803 Rüschlikon, Switzerland		
Phone:	+41 44 724 8061		
Fax:	-		
E-mail:	SAB@zurich.ibm.com		

Authors:	Stefan Abel, Johanna Nordlander, Felix Eltes, Jean Fompeyrine, Sébastien Cueff, Guillaume Saint-Girons, Ana Maria Gutierrez, Pau Castera, Alvaro Rosa, Pablo Sanchis, Regis Orobtchouk, Bertrand Vilquin, Pedro Rojo-Romeo, Domenico Tulli
Participants:	IBM, CNRS, UPVLC, DAS
Work Package	WP3
Estimated Person/month:	14
Security:	PU (Public)
Nature:	R (report)
Version:	1
Number of Pages:	18

ABSTRACT

A hybrid BTO/Si modulator device has been successfully designed to achieve a modulation bandwidth above 40GHz, a drive voltage below 2V, a modulation length below 2 mm and insertion losses below 5dB. The present report summarizes the designed device and reviews our recent progress on the experimental work. We solved the problem of high propagation losses in our BTO/Si slot waveguides and could thus fabricate and characterize various active devices. Specifically, devices based both on depositing amorphous silicon and on bonding crystalline silicon have been electro-optically characterized. From these measurements, we could observe electro-optical switching but it still remains to be proved that Pockels effect is the main switching mechanism.

1. Introduction

Within the framework of work package 3 of the SITOGA project, we develop active barium titanate / silicon photonic structures such as passive waveguides and active modulators based on ring resonators and Mach-Zehnder (MZ)-Interferometers. As specifications, the final MZ-modulators should have an electro-optical bandwidth above 40GHz, a V_π voltage below 2V, a modulation length below 2mm and an insertion losses below 5dB.

The present deliverable D3.5 is targeted to demonstrate $BaTiO_3$/Si Mach-Zehnder modulator compliant to the specifications. Due to unexpected high losses in passive structures and unforeseen features in the electro-optical (EO) response, we cannot show the ultimately targeted devices here. Instead, we provide a detailed update about our current results, including a description of the encountered issues and solutions of how to overcome them.

2. State-of-the-art of $BaTiO_3$/Si electro-optical devices

Table 1 lists an overview on the current state of the art of fabricated $BaTiO_3$ (BTO) based optical modulators/switches. For low-speed applications, partner IBM has shown ultra-low power tuning in the proposed BTO/Si waveguide structure with a tunability of 4 µW/nm [1]. A clear experimental demonstration of the Pockels effect in active $BaTiO_3$/Si waveguide devices has however not been provided by the previous publications [1], [2] and remains to be demonstrated.

Group	Orient.	Pol.	Structure	t_{BTO}	WG	V_π (measured)	$V_\pi L$ (V.cm)
IBM Research – Zurich Switzerland **[1]**	a/c-axis mixture	TM	SOI/$BaTiO_3$ 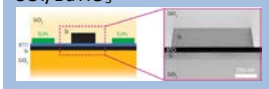	50nm (t_{Si}=70nm, t_{aSi}=220nm)	W=575nm	N/A	N/A
Yale University USA **[2]**	a-axis	TE	SOI/$BaTiO_3$ 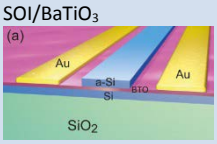	80nm (t_{Si}=t_{aSi}=110nm)	W=800nm L=750µm	20V@1550nm	1.5@1550nm
ISG1-IT Germany **[3]**	both	TE	$BaTiO_3$/MgO 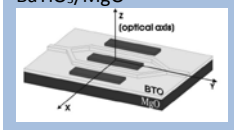	1µm (t_{slab}=50nm)	W=2µm L=3mm	c-axis: 8V@633nm 21V@1550nm a-axis: 6.3V@633nm 9.5V@1550nm	c-axis: 2.4@633nm 6.3@1550nm a-axis: 1.89@633nm 2.85@1550nm
Northwestern University USA **[4]**	c-axis	both	MgO/$BaTiO_3$/Si_3N_4 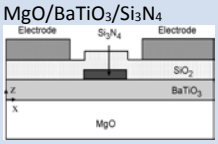	620nm (t_{Si3N4}=120nm)	W=2µm L=5mm	0.5V@973nm 1V@1561nm	0.25@973nm 0.5@1561nm

Table 1: State-of-the-art of experimentally demonstrated EO modulators based on $BaTiO_3$. The thickness values correspond to the thickness of the barium titanate film (t_{BTO}), of the etched waveguide slab (t_{slab}), of the silicon nitrate layer (t_{Si3N4}), of the amorphous silicon layer (t_{aSi}), and of the device silicon layer (t_{Si}), respectively.

Progresses have been made on simulations of the device performance of $BaTiO_3$/Si hybrid devices. Several groups in the US and in Europe (among the SITOGA partners UPVLC and INL) have investigated in detail the dependence of the electro-optical response on the device geometry and the orientation of the crystallographic domains [5]–[7]. Partner UPVLC has shown that *a*-axis

oriented barium titanate films show a stronger response compared to *c*-axis oriented films with in-plane electrodes. Furthermore, the influence of ferroelectric domain configuration on the performance of the devices has also been investigated [8].

3. Developed BTO/Si modulator in SITOGA

3.1. Final design of the BTO/Si modulator device

SITOGA target specifications require a modulation bandwidth above 40GHz, a drive voltage below 2V, a modulation length below 2 mm and insertion losses below 5dB. In order to achieve these specifications, the best electro-optical (EO) performance is obtained for single-domain *a*-axis oriented $BaTiO_3$ and TE polarization [6]. In this case, the V_π voltage can be significantly improved by rotating the waveguide structure with respect to the principal axes of $BaTiO_3$ at a certain angle. The variation of the V_π against the angle for TE and TM polarization is depicted in Figure 1(a).

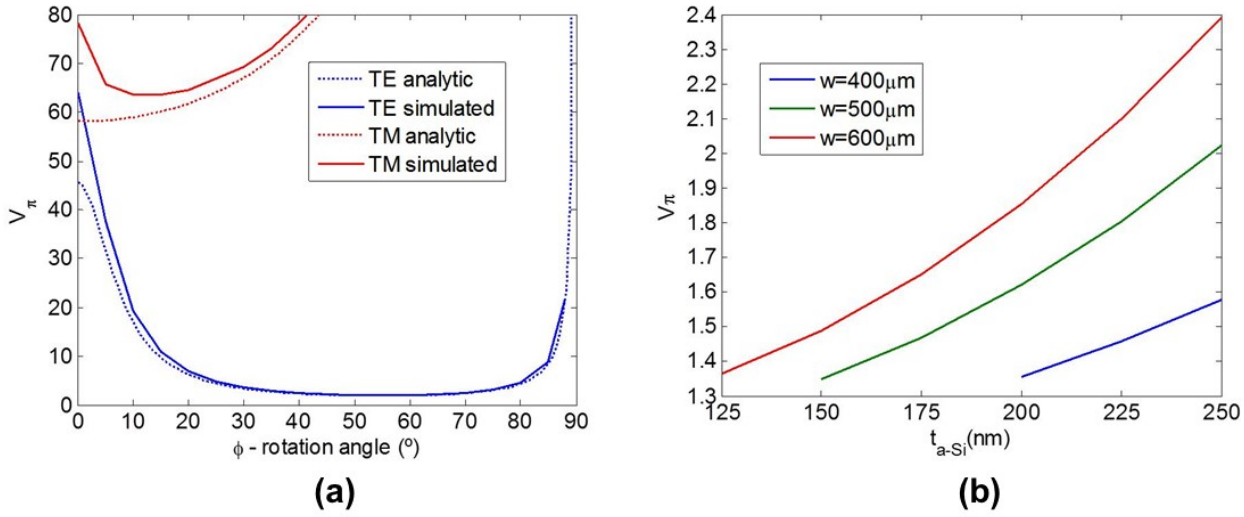

Figure 1: (a) V_π voltage as a function of the rotation angle for both polarizations and (b) V_π voltage for TE polarization at an angle of 55° as a function of the amorphous silicon thickness and a waveguide-to-electrode separation of 1μm.

The optimum EO performance is obtained for TE polarization and a rotation angle of 55°, for which a V_π voltage as low as 2V is achieved. Furthermore, this value can be decreased by optimizing the amorphous silicon thickness, waveguide width and waveguide-to-electrode separation. Figure 1(b) shows the V_π voltage as a function of the amorphous silicon thickness for different waveguide widths. It can be seen that a V_π voltage as low as 1.35V has been obtained for a modulation length of 2mm, i.e. $V_\pi L$ = 0.27 V·cm, at the optimum rotation angle of 55°.

In addition, EO simulations have been carried out to properly design the electrodes for high frequency operation. The results, shown in Figure 2, ensure that specifications can be accomplished. The high permittivity of $BaTiO_3$ (ε_z~56, ε_x~2200) reduces the RF impedance in comparison to usually lower dielectric constant substrates or thin films with symmetric coplanar waveguides.

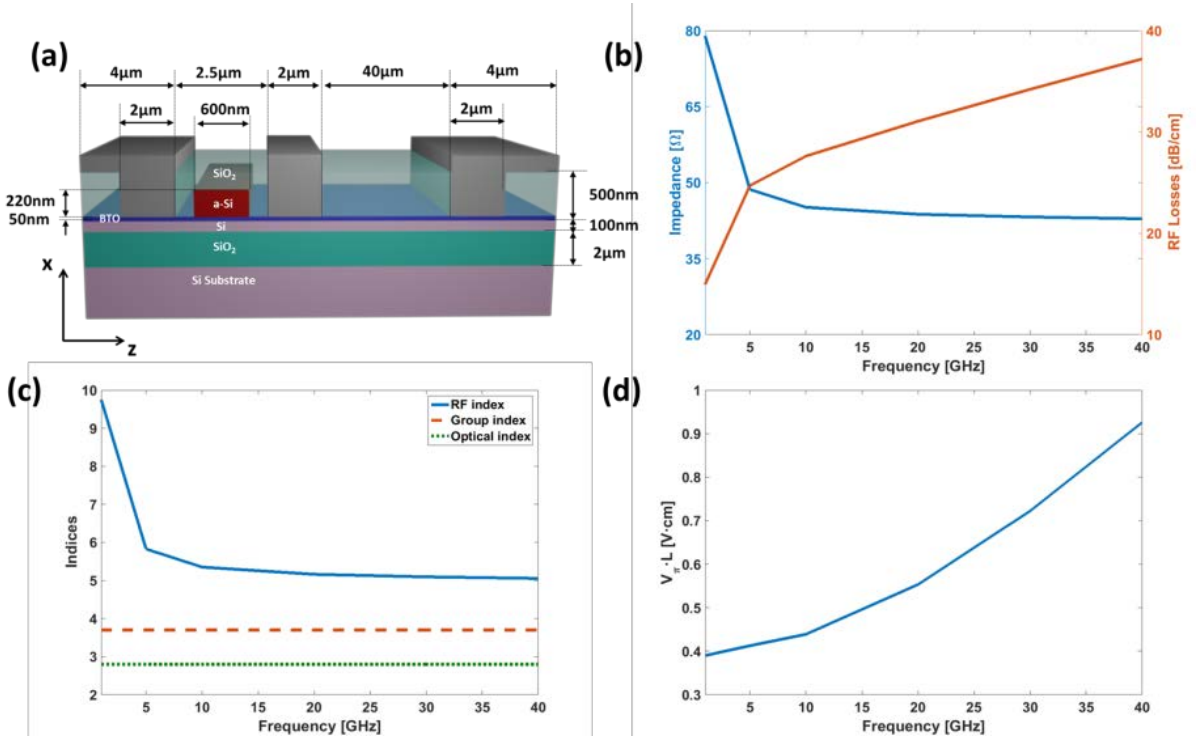

Figure 2: (a) Schematic of the waveguide cross-section showing the optimal parameters for a high RF performance. (b) RF impedance and losses, (c) RF, effective and optical group indices and (d) modulation efficiency as a function of the frequency.

In such a way, the electrode dimensions have been designed to overcome the high permittivity of $BaTiO_3$. Asymmetric coplanar electrodes, as those depicted in Figure 2(a), have been chosen to achieve a matching impedance around 50Ω, maintaining a narrow gap in the optical waveguide with the aim of keeping the modulation efficiency as high as possible. Figure 2(b) and (c) show the RF impedance and losses as well as the RF, effective, and optical group indices as a function of the frequency. It can be seen that the impedance is quite well matched. On the other hand, an EO bandwidth higher than 40 GHz is ensured as a result of the velocity matching between the electrical and optical signals. The modulation efficiency variation with the RF frequency is shown in Figure 2(d) with a $V_\pi L$ below 1V·cm ensured in the 40 GHz frequency range.

3.2. Devices based on depositing amorphous silicon

3.2.1. Passive measurements

The fabrication of the devices based on depositing amorphous silicon has been carried out at UPVLC by using the sputtered BTO/SOI samples provided by INL partner. Grating couplers have been designed and waveguides with different lengths have been used to measure the optical propagation losses. The main issue in a first step was to reduce the propagation losses. An enhancement has been obtained in each processed sample. This enhancement is mainly attributed to the decreased waveguides roughness and material granularity. The evolution of the measured propagation losses is shown in Figure 3.

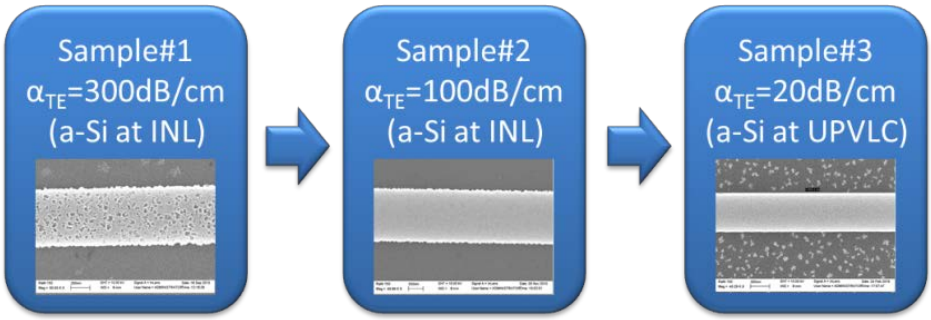

Figure 3: Schematic showing the reduction evolution in the measured propagation losses.

Apart from propagation losses, we have measured losses of 5.1dB for TE grating couplers in very good agreement with simulation results. Furthermore, focusing shaped gratings allow us to avoid the use of tapers and hence to reduce the footprint of devices.

3.2.2. DC measurements

After passive measurements, metallic electrodes were added at UPVLC, by windows opening, allowing the direct contact of the electrode with the BTO. SEM images of some fabricated structures with electrodes are shown in Figure 4. Ring resonators and Mach-Zehnder Interferometer (MZI) structures have been measured in the DC regime to analyze the electro-optical switching performance.

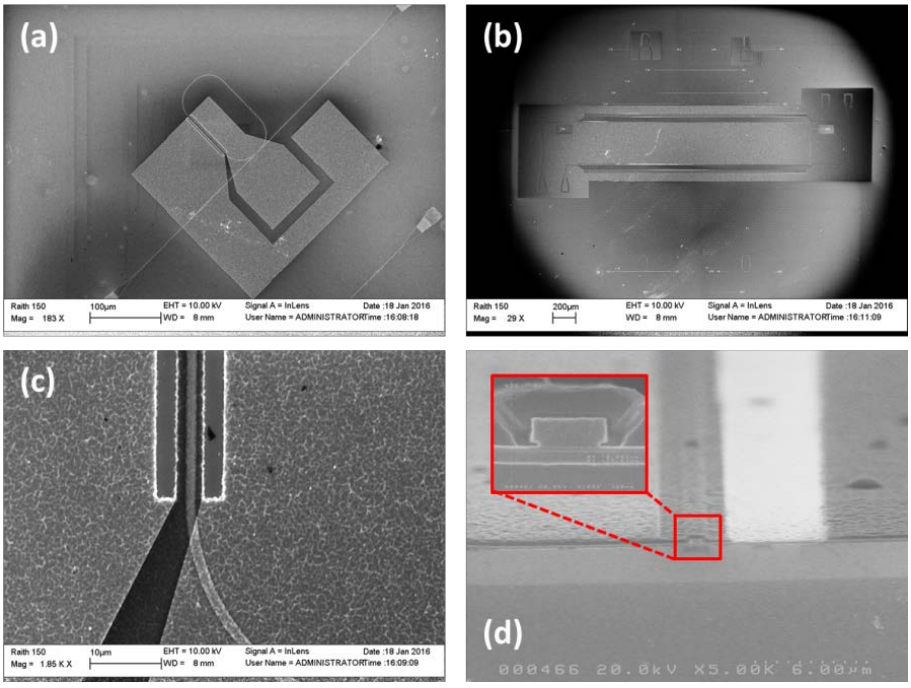

Figure 4: (a) Ring resonator modulator with lumped electrodes, (b) MZI modulator with travelling wave electrodes, (c) detail of opened windows in metallization process and (d) transversal profile of one arm of the MZI and inset a detail of the a-Si/BTO/Si waveguide.

In the case of the ring modulator, a modulation efficiency as low as $V_{\pi}L$=0.5Vcm has been estimated from DC measurements. However, for the 2mm-long MZI modulator (processed in another sample), a much lower modulation efficiency of 32Vcm was measured. Figure 5 shows the phase shift

as a function of the applied DC voltage for the (a) ring resonator and (b) MZI structure. By comparing both results it can be highlighted several issues:

- No hysteresis has been observed in any of the devices.
- The phase shift variation has different slopes depending on the voltage in both devices.
- The sign of the phase shift variation, and therefore of the effective index, for both structures is opposite when negative voltages are applied.

Therefore, it can be stated that although we have been able to see an electro-optical response, the obtained results are not in agreement with the expected performance for a modulation based exclusively on Pockels effect. Furthermore, we have also observed a large variability from sample to sample. In order to clarify the physical nature of the electro-optic response more experiments are required.

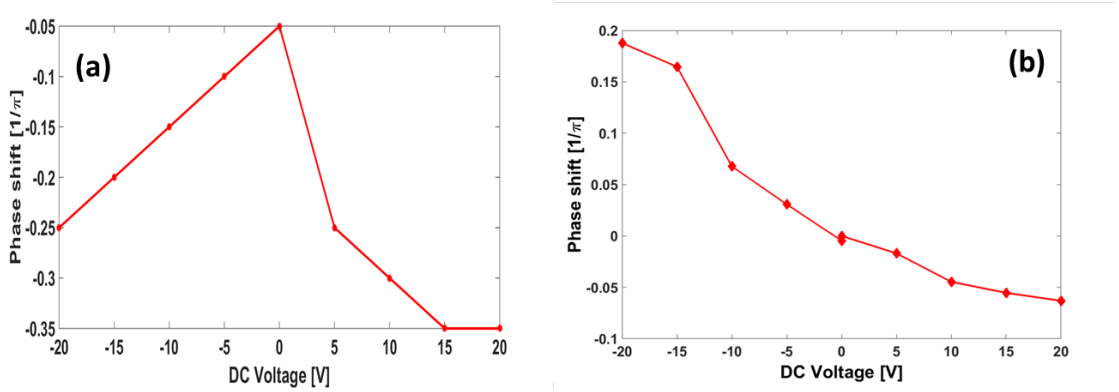

Figure 5: Phase shift as a function of the DC voltage for the (a) ring resonator and (b) MZI structures.

The IV response of the devices has also been characterized. Figure 6(a) show the response for the lumped electrodes used in the ring resonator. It can be seen that the leakage current is very low with values below 0.6µA. In this case, similar current values were also measured for the travelling-wave electrodes used in the MZI structure.

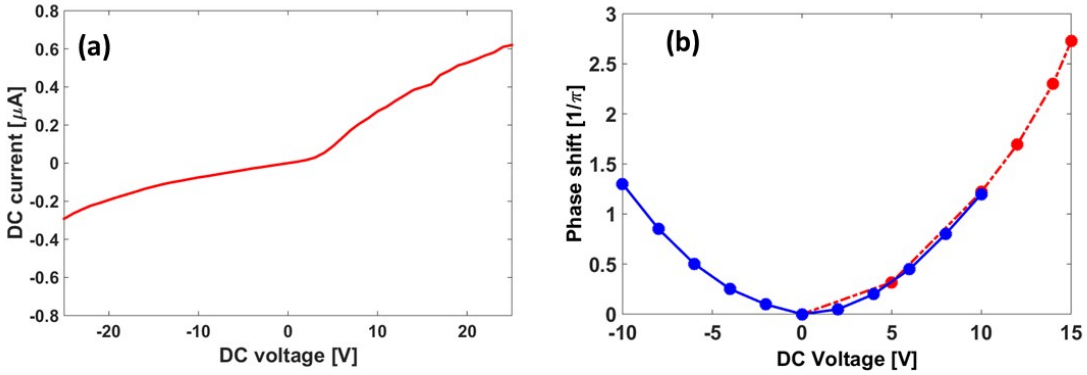

Figure 6: (a) IV curve obtained in the lumped electrodes of the ring resonator and (b) phase shift induced by short-circuiting the electrodes of the MZI structure.

On the other hand, the thermo-optic performance has also been analyzed. Figure 6(b) shows the phase shift variation as function of the applied voltage when the electrodes of the MZI structure were short-circuited. It can be seen that the reponse is not linear but the sign of the change is always positive ($\Delta n_{eff}>0$) for both positive and negative voltage values. The non-linearity is attributted to the different thermo-optic response of the materials (a-Si, BTO and c-Si) that form the optical waveguide and therefore are interacting with the optical mode.

3.2.3. AC measurements

For the moment, a low frequency modulation has only been succesfully observed at the ring resonator structure. We were able to measure up to 2MHz. The modulated optical signal is displayed in Figure 7(b). Higher RF frequency operation has not yet been possible. However, we think that mainly due to the too thin thickness of the metal electrodes (around 100nm) used in this sample.

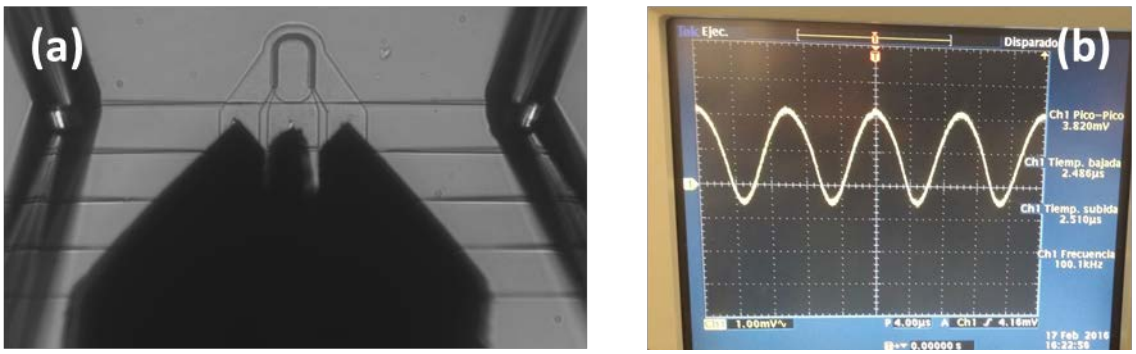

Figure 7: (a) Microscope image showing the RF probes and optical fibers while measurement of a ring resonator is being carried out and (b) output modulated signal measured at low frequency (f=100kHz).

New samples for testing both ring and MZI structures on the same sample are currently being fabricated. Furthermore, with respect to the first processed samples, we expect that thicker electrodes will improve the RF performance. Furthermore, the lower propagation losses will also help to achieve a better modulation performance.

3.3. Devices based on bonding crystalline silicon

As a complementary route to fabricating hybrid $BaTiO_3$/Si slot waveguides using an amorphous silicon layer (section 3.2), we continued the approach to use crystalline silicon as top-silicon layer. The integration of this crystalline silicon layers is performed via molecular bonding, as described in previous deliverables (D3.2, D3.4). We advanced our investigation on the reduction of propagation losses in passive structures and on the electro-optic response of active devices, and provide updates with new insights in the following sections.

3.3.1. Reduction of propagation losses in passive devices

In D3.4, we already reported on the reduction of the initially very high propagation losses (>100 dB/cm) to low values of ~7 dB/cm in passive $BaTiO_3$/Si slot waveguides. We continued our study to identify the physical origin of the initially high losses, and our efforts to define a stable process to permanently reduce the source of the losses.

Indeed, we could identify the $SrTiO_3$ seed layer in the $BaTiO_3$/$SrTiO_3$/Si stack as the major source of propagation losses in hybrid waveguides. We could also clearly define a new waveguide fabrication route that reduces these losses to values of only few dB/cm with special annealing procedures in a reliable way. As a result, we are now able to fabricate long waveguides as necessary for MZIs and ring resonators with high quality factors (Figure 8). We summarized our findings in a manuscript that has been submitted to a peer-reviewed journal.

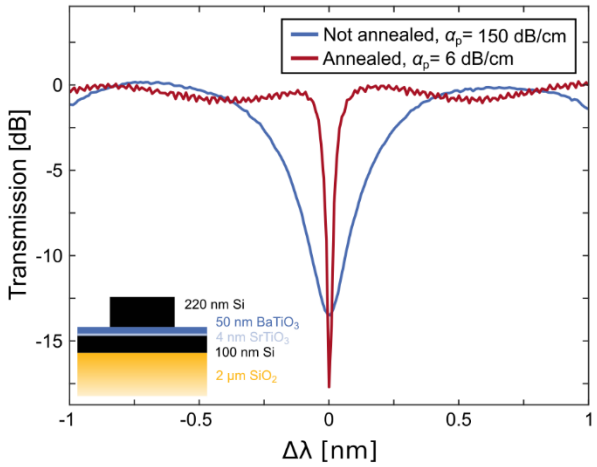

Figure 8: Comparison of ring resonator spectra before and after annealing. The spectra are taken from ring resonators with a 75 µm radius and gap sizes close to critical coupling. The spectra are normalized to account for insertion losses. The inset illustrates the waveguide cross section.

3.3.2. EO response of active devices

Previously, we delivered results on the EO response of Si/$BaTiO_3$/Si slot waveguides with crystalline top silicon layers (D3.4). While we could observe a shift of the resonance wavelength of ring resonators when applying a voltage, the properties of these shifts are also not in full agreement with the expected performance for devices with the Pockels effect as the origin of the EO switching. Examples of such unexpected features are long-term drifts, changes in the extinction ratio, and asymmetric hysteretic behavior.

We continued our work on identifying the physical origin of the observed EO switching behavior by characterizing various devices with different layer stacks and different geometries. Figure 9 shows some examples of devices fabricated for these experiments with varying gap size between the electrodes (Figure 9 left) and different device layouts such as race track resonators (Figure 9 right).

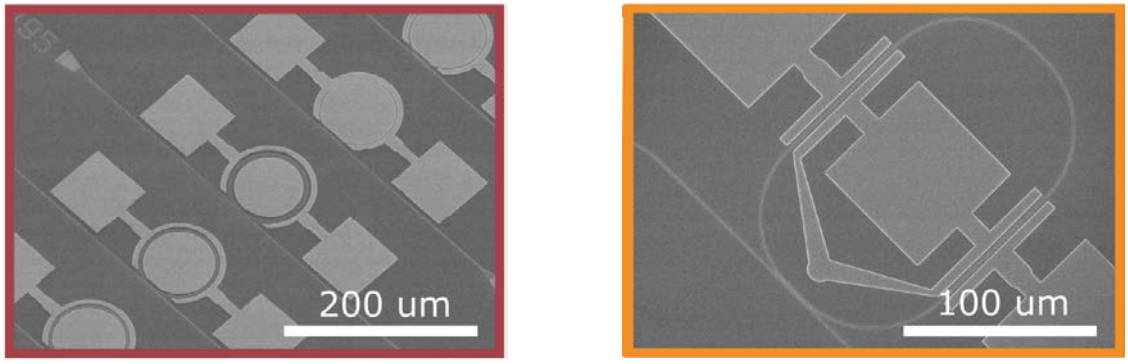

Figure 9: SEM images of devices investigated to identify the switching mechanism. Left: Ring resonators with various electrode geometries. Right: Racetrack resonator.

We characterized the devices with slowly varying applied voltages. Therefore, we coupled light into the devices using a fiber optical setup, and measured the transmission spectrum with an optical spectrum analyzer. For extracting the electro-optical response, we measured these spectra for differently applied voltages. The full setup is shown in Figure 10 with additional explanations in the figure caption. The speed of voltage variations is limited by the time needed to record a full optical spectrum, which is ~4 s. We evaluated the data by fitting the resonance wavelength, and determining the relative changes of the mode indices in order to compare devices with different ring radii.

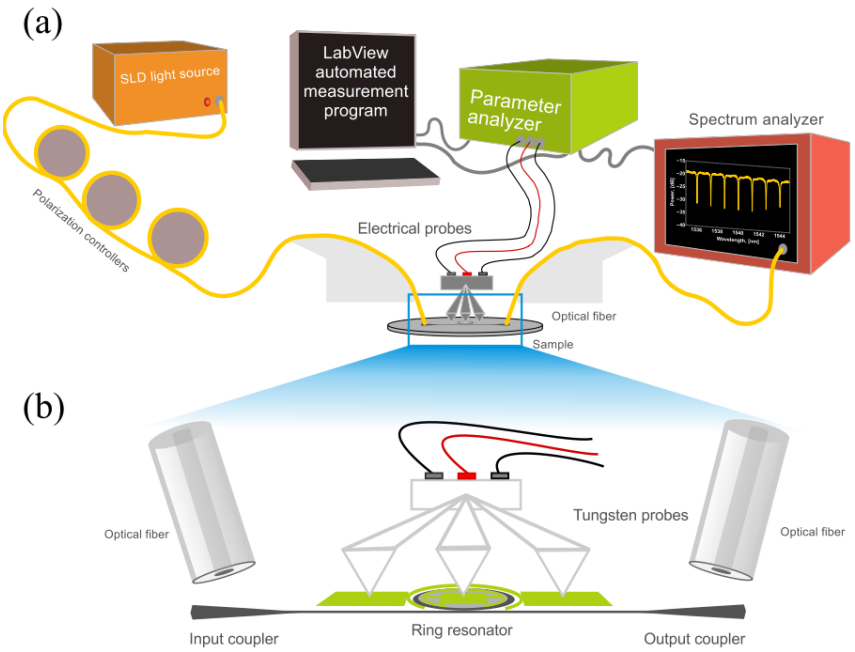

Figure 10: Schematic illustrating the optical and electro-optical setup used for characterizing $BaTiO_3$ slot waveguides with crystalline top silicon layers. (a) The optical measurement system with fiber optics coupled to the devices on the sample. The polarization of the light from the SLED light source is controlled through polarization controllers. The transmitted optical power is recorded by a spectrum analyzer. (b) For the electro-optical measurements the setup is extended with a parameter analyzer tool connected to electrical probes.

By comparing different waveguide structures, we could identify a strong impact of the actual processing route on the electro-optical response. An example of this impact is shown in Figure 11, where the change of the mode index and the leakage current is shown for two samples. Different direct bonding conditions are the main distinction between the two samples. As clearly visible in Figure 11, the bonding conditions have a strong impact on the magnitude of the electro-optical response, the shape of the hysteresis loop, and the reproducibility of the data. While we could already link certain processing steps and material properties to the electro-optical response, our study on identifying the electro-optical switching mechanism is still ongoing and has not been concluded yet.

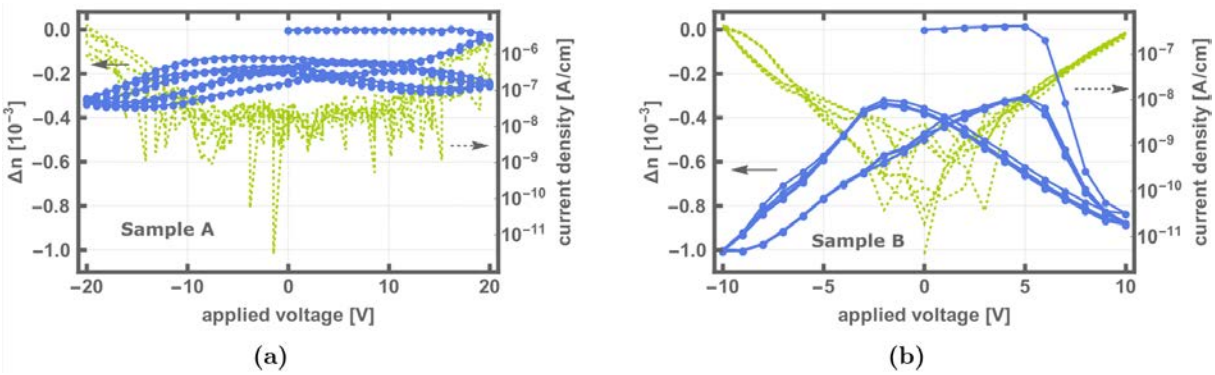

Figure 11: Electro-optical response and leakage current (normalized by electrode length) from sweeping the voltage. (a) and (b) show the response of two differently processed samples. The poling event in sample B is reversible and observed in all characterized devices.

4. Conclusion

A hybrid BTO/Si waveguide structure modulator device has been successfully designed for optimum EO performance in order to achieve SITOGA specifications consisting in a bandwidth above 40GHz, a drive voltage below 2V, a modulation length below 2 mm and insertion losses below 5dB.

Experimentally we could not demonstrate devices with such characteristics yet. The major reasons for this are unexpected high propagation losses, which delayed our progress significantly. However, we were able to identify the sources of the losses and reduce them significantly to <10 dB/cm. Only this reduction of the losses allowed us to continue with fabricating active devices. Indeed, we could realize active devices for both fabrication routes followed in the SITOGA project, namely with amorphous and crystalline top-silicon layer. With both types of devices we could indeed observe electro-optical switching. However, the characteristics of the response does not match the expected behavior of Pockels-effect-based switching.

Therefore, we are now focusing on identifying the source of the physical switching mechanism to ultimately remove other, non-Pockels effect electro-optical switching paths, and thus to demonstrate devices that meet the specifications targeted in SITOGA. We could already identify various processes and device features as sources for the deviation in the expected and observed electro-optical characteristics, such as the influence of the bonding step or the thickness of the metal pads. However, a final conclusion cannot be provided at this time without further results from our ongoing experimental investigations.

5. References

[1] S. Abel, T. Stöferle, C. Marchiori, D. Caimi, L. Czornomaz, M. D. Rossell, R. Erni, M. Sousa, H. Siegwart, B. J. Offrein, and J. Fompeyrine, "Barium-titanate integrated with silicon photonics for ultra- efficient electro-optical performance," in *ECOC proceeding*, 2015, p. 0556.

[2] C. Xiong, W. Pernice, J. Ngai, J. Reiner, D. Kumarh, F. Walker, C. Ahn, and H. Tang, "Active silicon integrated nanophotonics: ferroelectric $BaTiO_3$ devices," *Nano Lett.*, vol. 14, no. 3, pp. 1419–1425, 2014.

[3] A. Petraru, J. Schubert, M. Schmid, and C. Buchal, "Ferroelectric $BaTiO_3$ thin-film optical waveguide modulators," *Appl. Phys. Lett.*, vol. 81, no. 8, p. 1375, 2002.

[4] P. Tang, A. L. Meier, and D. J. Towner, "$BaTiO_3$ thin-film waveguide modulator with a low voltage – length product at near-infrared wavelengths of 0 . 98 and 1 . 55 mm," *Opt. Lett.,* vol. 30, no. 3, pp. 254–256, 2005.

[5] W. H. P. Pernice, C. Xiong, F. J. Walker, and H. X. Tang, "Design of a Silicon Integrated Electro-Optic Modulator Using Ferroelectric $BaTiO_3$ Films," *J. Light. Technol.*, vol. 26, no. 13, pp. 1344–1347, 2014.

[6] P. Castera, D. Tulli, A. M. Gutierrez, and P. Sanchis, "Influence of $BaTiO_3$ ferroelectric orientation for electro-optic modulation on silicon," *Opt. Express*, vol. 23, no. 12, p. 15332, 2015.

[7] X. Hu, S. Cueff, P. R. Romeo, and R. Orobtchouk, "Modeling the anisotropic electro-optic interaction in hybrid silicon-ferroelectric optical modulator," *Opt. Express*, vol. 23, no. 2, p. 1699, 2015.

[8] P. Castera, A. M. Gutierrez, D. Tulli, Sébastien Cueff, Regis Orobtchouk, Pedro Rojo Romeo, Guillaume Saint-Girons and P. Sanchis, "Electro-Optical Modulation Based on Pockels Effect in $BaTiO_3$ With a Multi-Domain Structure," *IEEE Photonics Technology Letters*, vol. 28, no. 9, pp. 990-993, 2016.